

## Study of the effects of guide field on Hall reconnection<sup>a)</sup>

T. D. Tharp,<sup>1,b)</sup> M. Yamada,<sup>1</sup> H. Ji,<sup>1</sup> E. Lawrence,<sup>1</sup> S. Dorfman,<sup>1</sup> C. Myers,<sup>1</sup> J. Yoo,<sup>1</sup> Y.-M. Huang,<sup>2</sup> and A. Bhattacharjee<sup>2</sup>

<sup>1</sup>Center for Magnetic Self-Organization, Princeton Plasma Physics Laboratory, P.O. Box 451, Princeton, New Jersey 08543-0451, USA

<sup>2</sup>Space Science Center, University of New Hampshire and Max Planck-Princeton Research Center for Plasma Physics, Princeton University, P.O. Box 451, Princeton, New Jersey 08543-0451, USA

(Received 16 November 2012; accepted 3 April 2013; published online 16 May 2013)

The results from guide field studies on the Magnetic Reconnection Experiment (MRX) are compared with results from Hall magnetohydrodynamic (HMHD) reconnection simulation with guide field. The quadrupole field, a signature of two-fluid reconnection at zero guide field, is modified by the presence of a finite guide field in a manner consistent with HMHD simulation. The modified Hall current profile contains reduced electron flows in the reconnection plane, which quantitatively explains the observed reduction of the reconnection rate. The present results are consistent with the hypothesis that the local reconnection dynamics is dominated by Hall effects in the collisionless regime of the MRX plasmas. While very good agreement is seen between experiment and simulations, we note that an important global feature of the experiments, a compression of the guide field by the reconnecting plasma, is not represented in the simulations.

© 2013 AIP Publishing LLC. [<http://dx.doi.org/10.1063/1.4805244>]

### I. INTRODUCTION

Magnetic reconnection,<sup>1,2</sup> a fundamental plasma physics process in which magnetic fields of opposite direction break and reconnect, can be significantly influenced by the presence of a third component of magnetic field, known as a guide field, which is perpendicular to the reconnection plane (see Figure 1).

Most instances of reconnection in nature<sup>3–5</sup> and the laboratory,<sup>6–12</sup> which have been studied both analytically and numerically<sup>13–25</sup> by means of 2.5-dimensional models, contain a significant guide field ( $B_g$ ) in comparison with the reconnecting magnetic field strength ( $B_{rec}$ ). In magnetosphere reconnection,<sup>3,4</sup> for example, guide fields often reach the level of the reconnecting field ( $B_g \sim B_{rec}$ ), while reconnection in fusion experiments (such as during tokamak<sup>26</sup> or reversed-field pinch<sup>27</sup> sawteeth) can have guide fields exceeding  $20B_{rec}$ .

Sweet<sup>28</sup> and Parker<sup>29</sup> offered the first quantitative description of magnetic reconnection to explain astrophysical observations. While applicable to collisional plasmas,<sup>30</sup> their model fails to reproduce the fast reconnection rates observed in collisionless plasmas. In the collisionless regime, fast reconnection can be modeled by treating the electrons and ions as two independent fluids. In two-fluid reconnection, Hall effects allow the plasma to achieve fast reconnection and typically produce a characteristic quadrupole field,<sup>31</sup> illustrated (without a guide field) in Figure 1. Previous Magnetic Reconnection Experiment (MRX) results without a guide field<sup>32</sup> showed that the local reconnection dynamics are dominated by Hall effects in the collisionless regime when the thickness of the reconnection layer is less than the electron mean free path. The present results are an

extension of this research to include reconnection with a guide field, and the results are consistent with previous MRX results in the collisionless regime. To date, there is no consensus model able to analytically quantify the dependence of the reconnection rate on guide field strength for a two-fluid plasma. However, simulations (e.g., Refs. 17–22) routinely show that the two-fluid reconnection rate is reduced by the presence of guide field.

Presently, we report on the systematic investigation of guide field effects on a laboratory plasma. A toroidal guide field has been applied to reconnection plasmas in the MRX using an external, steady-state toroidal field (TF) coil, resulting in a modification of the quadrupole fields and a reduction of the reconnection rate.<sup>33</sup> We compare these results with Hall magnetohydrodynamic (HMHD) simulation, and find good agreement in the quadrupole field structure and reconnection rate. In both experiment and simulation, the reconnection rate

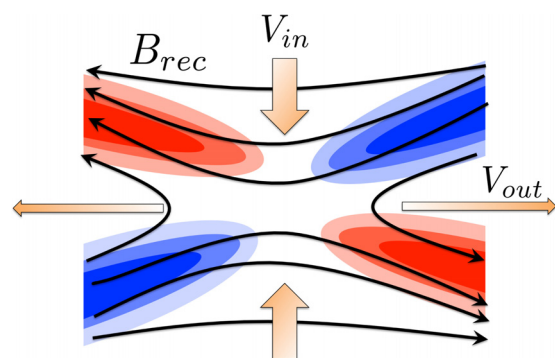


FIG. 1. A typical reconnection geometry illustrating the reconnecting magnetic field ( $B_{rec}$ ), the flow pattern ( $V_{in}$  and  $V_{out}$ ), and the out-of-plane quadrupole field (shaded region). The coloring indicates that for zero guide field plasmas, the quadrupole field is directed into (blue) or out-of (red) the reconnection plane. The guide field and reconnection electric field are also directed perpendicular to the plane.<sup>2,32,36</sup>

<sup>a)</sup>Paper T12 6, Bull. Am. Phys. Soc. 57, 293 (2012).

<sup>b)</sup>Invited speaker.

is reduced in parallel with a reduced magnitude of the Hall term of Ohm's law. The reconnection rate in the experiment is also impacted by a global compression of the applied guide field. In addition to enhancing the local value of the guide field, we observe a correlation between the measured reconnection rate and the magnetic pressure associated with the compressed field in the reconnection outflow. We postulate that this may also impact the reconnection rate by modifying the boundary conditions for the local reconnection dynamics.

## II. MRX DEVICE

In MRX, plasmas are formed by a combination of poloidal field (PF) coils and TF coils embedded within two toroidally symmetric flux cores. The PF coils are toroidally wound wires and produce the in-plane reconnecting field, as illustrated in Figure 2. By quickly reducing the PF coil current, reconnection is driven with radial inflow and axial outflow in a mode of operation known as "pull reconnection."

The TF coil is helically wound within the flux core and produces a time-varying toroidal field inside the flux core; this, in turn, produces a poloidal electric field outside the flux core, which is used to break down the fill gas into a plasma. We make use of two operational modes of MRX: counterhelicity, in which the TF coils have opposite polarity, and cohelicity, in which the TF coils have the same polarity. In counterhelicity operation, the TF coils drive current locally near the flux cores, resulting in a reconnection region with nearly zero guide field. In cohelicity operation, the toroidal field coils drive a global circulation of plasma current linking the two flux cores, thus producing a strong toroidal field throughout the reconnection region. By combining the two modes of operation with an independently applied guide field produced by an external coil wrapped through the center column of MRX, we can experimentally span a range of guide fields of roughly  $-3B_{rec} < B_g < 3B_{rec}$ .

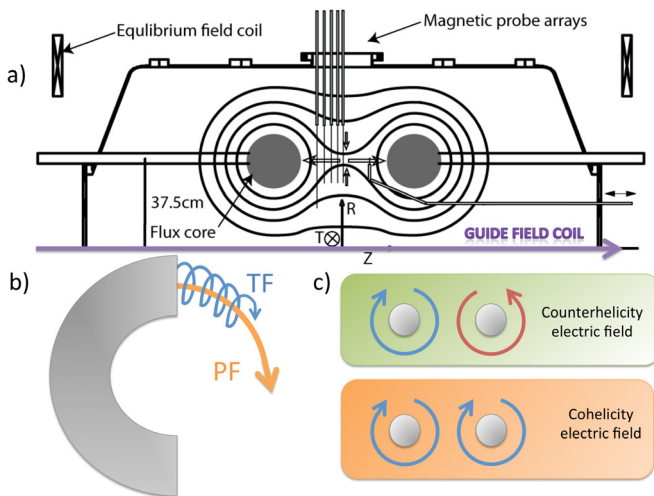


FIG. 2. A schematic of MRX. (a) The picture shown is a cross-section of the cylindrically symmetric vacuum vessel with magnetic field lines drawn. The toroidal direction is out of the plane. (b) Each flux core contains a PF winding to produce the magnetic x-point geometry and a TF helically wound coil, which produces an electric field used to break down the plasma. (c) The two modes of MRX operation produce plasmas with little residual guide field (counterhelicity) and a large residual guide field (cohelicity).

The magnetic field is measured using more than 300 magnetic pickup coils inserted into the plasma. By measuring magnetic field globally, we directly measure the reconnection rate as  $E_\phi = -\frac{1}{2\pi r} \frac{\partial \psi}{\partial t}$ , where  $\psi(r) = 2\pi \int_0^r B_z r' dr'$  is the poloidal flux. This measurement is based on an assumption of toroidal symmetry; although MRX plasmas are not perfectly symmetric, the plasma asymmetry does not result in a substantial error in our measurement. We use a Harris sheet fit<sup>34,35</sup> to identify the magnitude of the reconnecting field,  $B_z \sim B_{rec} \tanh(r/\delta)$ . Electron density and temperature are measured near the center of the reconnection layer using a Langmuir probe. The plasma is formed using deuterium gas filling the vacuum vessel to a pressure of a few milliTorr.

Measurements indicate that the plasmas under consideration are in a two-fluid regime,<sup>1,2,32</sup> with the current sheet half width ( $\delta \sim 2$  cm) smaller than the ion skin depth ( $c/\omega_{pi} \sim 5$  cm) and of comparable scale to the ion sound gyroradius ( $\rho_s \sim 2.5$  cm).<sup>18</sup> A strong signature of two-fluid physics is the out-of-plane quadrupole field,<sup>35,36</sup> which is readily identifiable in zero guide field plasmas.

## III. QUADRUPOLE FIELD STRUCTURE

As the guide field is increased during counterhelicity operation, the quadrupole field is modified, but still present, even for  $B_g \sim B_{rec}$ . The quadrupole field is not easily experimentally identified during cohelicity operation, because it is difficult to distinguish the two-fluid Hall field from the natural spatial variation of the guide field; thus, we limit the discussion about quadrupole field to plasmas produced using the counterhelicity mode.

We compare these measurements with numerical simulations carried out in a domain of the size  $L_x \times L_z$ , with  $L_x = 25d_i$  and  $L_z = 12.5d_i$ , utilizing periodic boundary conditions in  $x$  and perfectly conducting boundaries in  $z$ . The initial magnetic field is a standard Harris sheet profile with a uniform guide field, with a small perturbation added to initiate reconnection. In normalized units,

$$B_x = \tanh(z/h) - \epsilon \frac{L_x}{2L_z} \cos\left(\frac{2\pi x}{L_x}\right) \sin\left(\frac{\pi z}{L_z}\right),$$

$$B_y = B_g, \text{ and}$$

$$B_z = \epsilon \sin\left(\frac{2\pi x}{L_x}\right) \cos\left(\frac{\pi z}{L_z}\right),$$

where  $h$  is the initial current sheet width and  $\epsilon$  is a small parameter. Here, we take  $h = 0.5d_i$  and  $\epsilon = 0.05$ . The initial density profile is  $\rho = 1 + 1/4T_0 \cosh^2(z/h)$ , and the pressure is  $p = 2\rho T_0$ , where  $T_0 = 0.125$  is chosen. We assume electron and ion temperatures to be equal, and the pressure is evolved adiabatically with the ratio of specific heat  $\gamma = 5/3$ . The plasma resistivity  $\eta$  is set to 0.005 to break the frozen-in condition, which corresponds to  $S_{d_i} = 200$ , where  $S_{d_i} = d_i V_A / \eta$  is the Lundquist number using  $d_i$  as the length scale. All the measurements are carried out when the reconnection rate reaches its peak.

Figure 3 shows contours of the measured out-of-plane field,  $B_g$ , for five MRX discharges with different values of

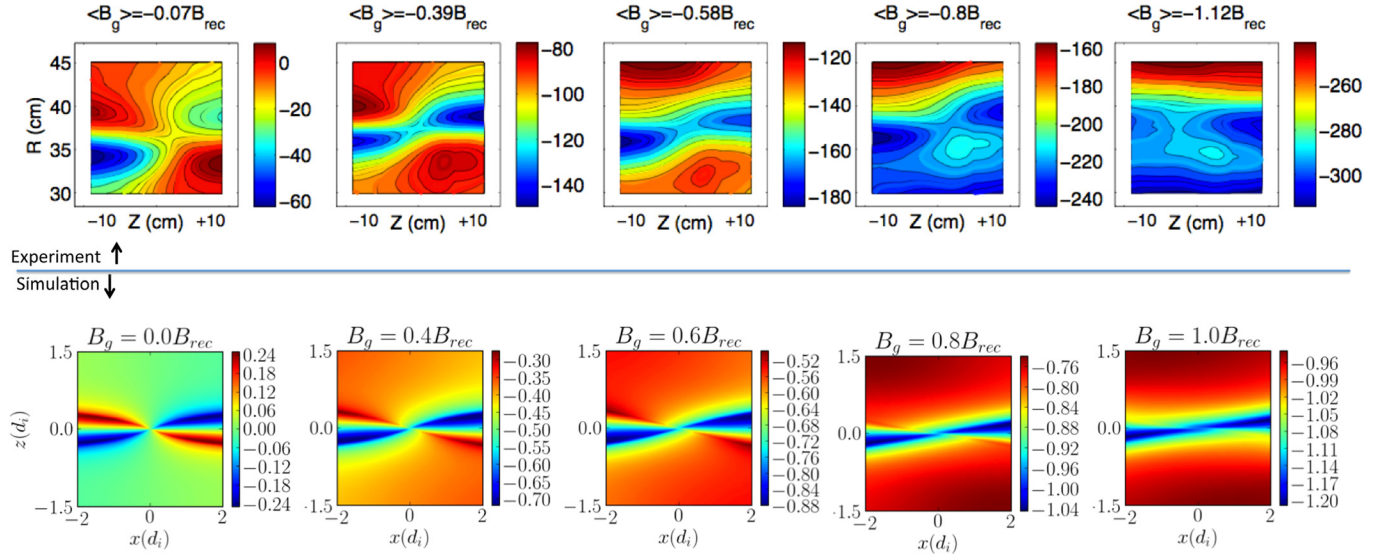


FIG. 3. Top: Contours of the toroidal field for measured guide fields spanning  $B_g \sim 0$  (left) to  $B_g \sim B_{rec}$  (right) during counterhelicity operation. Bottom: Quadrupole field patterns produced using Hall-MHD simulation. Note that the contour scales are independently determined for each plot to maximize contrast; for a discussion of the relative quadrupole field amplitudes, see Figure 4 and associated text. The contours have been plotted with the same spatial scale between simulation and experiment, setting  $d_i = 5$  cm.

applied guide field in the upper row of plots, and corresponding cases of HMHD simulation in the lower row of plots. There are some discrepancies between experiment and simulation, including a slight disagreement in the size of the quadrupole lobes, and a superimposed radial structure present in high guide field experimental data, which is absent in the simulation. In general, however, the shape of the quadrupole field is modified very similarly in experiment and simulation as the guide field is increased. We interpret the qualitative similarity seen here (at least in the first four frames) as physical evidence supporting the conclusion that interactions between the Hall currents and the applied guide field result in a modified electron flow and the associated quadrupole field structure.

#### IV. RECONNECTION RATE

In addition to a changing quadrupole field structure, both experiment and simulation observe a reduced reconnection rate and a reduced quadrupole field amplitude (or equivalently, a reduced Hall current) as guide field is increased. These two quantities are related by the out-of-plane Ohm's law for steady-state two-fluid reconnection.<sup>32</sup> Slightly upstream and downstream of the x-point, the ion flow contribution and the resistive term of Ohm's law are small, such that

$$E_{rec} \approx \left( \frac{J_r B_z}{ne} \right)_{\text{inflow}} \approx \left( \frac{J_z B_r}{ne} \right)_{\text{outflow}}.$$

In Figure 4(a), we show measurements of  $E$  and  $J \times B$ , where  $J_r$  and  $B_z$  are measured 4 cm upstream of the x-point (in the inflow region), while  $J_z$  and  $B_r$  are measured 8 cm downstream of the x-point (in the outflow region), roughly corresponding to the locations of maximum Hall term. We normalize the reconnection electric field to  $B_{rec} V_A$ , where  $B_{rec}$  is the magnitude of the reconnecting field

( $z$ -component), and  $V_A = B_{rec} / \sqrt{\mu_0 m_i n_i}$  is the Alfvén speed calculated using  $B_{rec}$ . (This is a typical normalization because the Sweet-Parker reconnection rate<sup>28,29</sup> is given by  $\frac{V_{in}}{V_A} = \frac{E_{rec}}{B_{rec} V_A}$ .) The corresponding values for the simulation are shown in Figure 4(b). Here, we plot a simulated “measurement” at the location of the maximum Hall term contribution. The scaling of the reconnection rate with the Hall term, taken together with the modified quadrupole field structure, is suggestive a physical mechanism for the reduced reconnection rate: The applied guide field intersects the path of electron flow, reducing the inflow Hall term,  $J_r B_z / ne$ , and thereby reducing the reconnection rate.

Despite the very good agreement between Figures 4(a) and 4(b), some care should be taken in the quantitative comparison of these results. While we have tuned the parameters of our simulation to match MRX conditions as accurately as possible, this slab geometry still fails to capture some important aspects of the true boundary conditions of MRX reconnection, so the quality of the agreement between experiment and simulation should be taken with a grain of salt.

#### V. GLOBAL EFFECTS OBSERVED IN MRX

Next, we present observations that the reconnection rate in MRX may also be impacted by magnetic pressure associated with the compression of guide field on large scales. A global circulation of current flowing around the MRX flux cores results in a larger guide field in the outflow region of the reconnection than the inflow. This results in a higher magnetic pressure in the plasma outflow than the upstream region, and the magnitude of this pressure imbalance is large enough that it cannot be ruled out as an important contributing factor to the reconnection rate. This pileup of magnetic pressure is due to the large-scale global geometry of the MRX experiment, and it is not accurately modeled by the boundary conditions of the simulation.

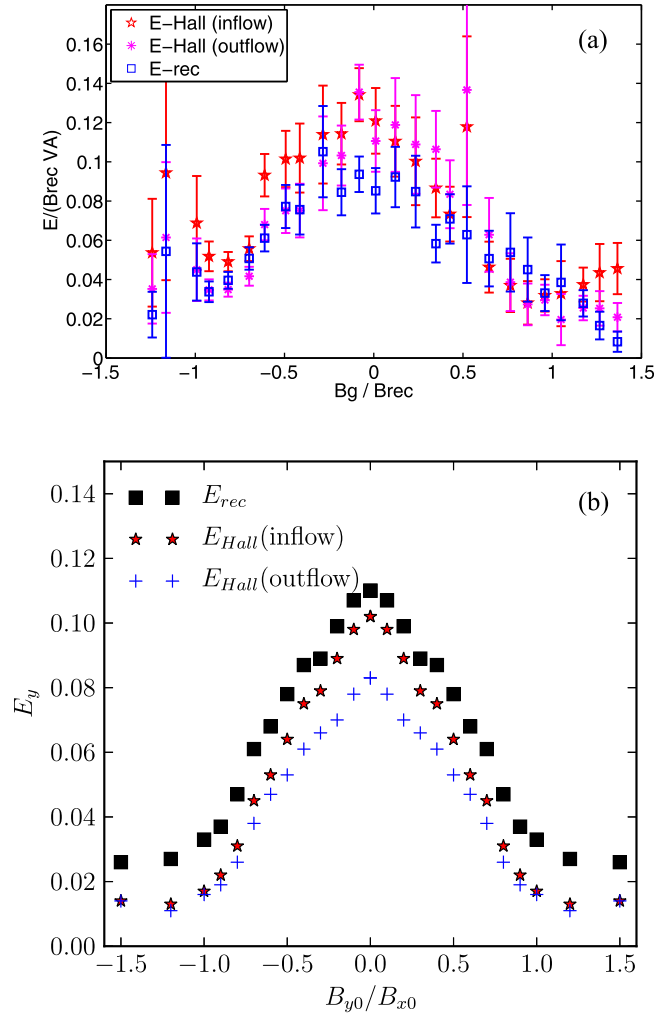


FIG. 4. Reconnection electric field ( $E_{rec}$ ) and the “Hall Electric Field” ( $\frac{J \times B}{ne}$ ) versus normalized guide field,  $B_g/B_{rec}$ . (a) Measurements of  $J_r \times B_z/ne$  measured 4 cm upstream of the x-point (labeled “inflow”) and  $J_z \times B_r/ne$  measured 8 cm downstream of the x-point (labeled “outflow”). Error bars denote the statistical variance over multiple shots. The density is measured in a single location near the center of the reconnection layer. (b) Simulation “measurements” of the reconnection electric field and the Hall terms. The measurement is taken at the location of the peak Hall term contribution.

A full-scale radial profile of the guide field in a typical counterhelicity MRX plasma is illustrated in Figure 5(a). At  $z=0$ , the guide field is peaked at the radial position of the current sheet, effectively amplifying the applied guide field for reconnection studies. Note that the spatial structure of the resulting enhanced guide field has a characteristic scale ( $\sim 20$  cm) that is much larger than the scales of the reconnection layer ( $\sim 5$  cm). Detailed measurements in MRX, such as those shown in Figures 3 and 4, only cover a narrow region centered near the x-point, which is also the approximate location of maximum guide field. Hence, the value of guide field at the reconnection x-point was used as the guide field value in the previous analysis.

In Figure 5(b), we show the measured guide field at the reconnection layer as a function of the applied guide field for both counterhelicity and cohelicity plasmas. The measured guide field is larger than the applied field for all cases, but the degree of enhancement is different for the two modes of operation. Counterhelicity and cohelicity plasmas are

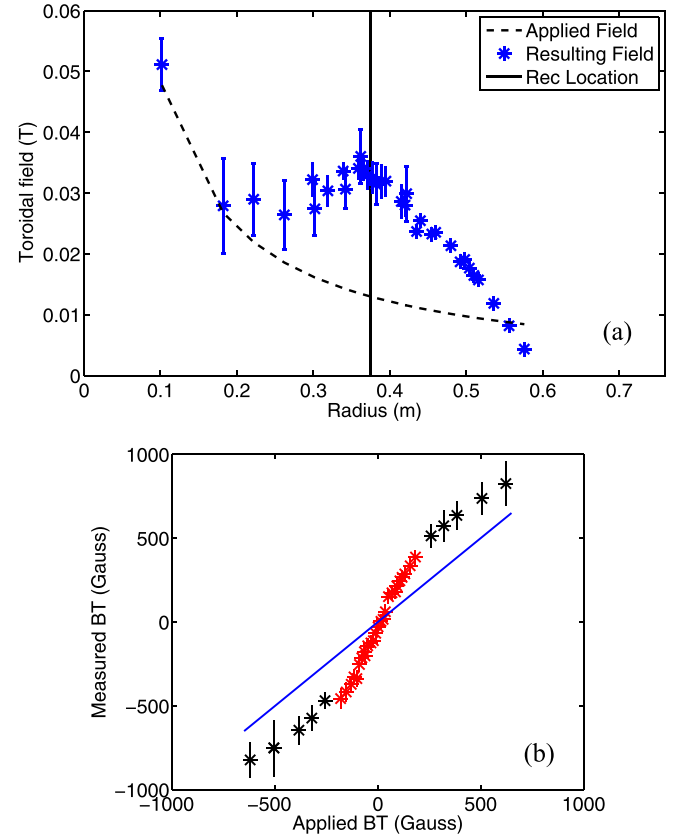


FIG. 5. Guide field pileup as a function of (a) radius, and (b) applied field. (a) Typical toroidal field profile measured at  $z=0$  and spanning over most of the MRX radius during counterhelicity reconnection with an externally imposed guide field, resulting in a total guide field at the reconnection layer of  $B_g \approx 1.2B_{rec}$ . The quadrupole field measurements in Figure 3 are made near the peak value of the compressed toroidal field, between  $r = 0.3$  and  $0.45$ . (b) Measured guide field at the reconnection x point as a function of the applied guide field at this position. The guide field enhancement depends on the operational mode of MRX: in counterhelicity plasmas (red: points with applied field  $|B_g| < 250$  Gauss), the enhancement roughly doubles the applied field, while cohelicity operation (black: points with applied field  $|B_g| > 250$  Gauss) results in a nearly constant offset in addition to the applied field.

produced with different startup methods and flux core currents, and therefore comparisons such as Figure 5(b) should not be interpreted as a smooth scan from zero guide field to the maximum guide field ( $3B_{rec}$ ).

In addition to increasing the effective guide field for reconnection studies, guide field compression can play a role in the reconnection dynamics by modifying the boundary conditions of the reconnection. In particular, we observe in MRX that this guide field produces a stronger magnetic pressure in the reconnection outflow region than the inflow, and therefore may contribute to the reconnection rate reduction.

The applied toroidal field is constant in time and varies as  $B_{applied} \sim 1/R$ . This vacuum field does not exert a force on the plasma (magnetic pressure and tension exactly cancel), indicating that the applied field alone does not meaningfully contribute to the plasma pressure balance. However, the pressure associated with the compressed field,  $B_\phi - B_{applied}$ , can contribute a net magnetic force. Note that this pressure description is only an approximation of the true magnetic forces in MRX since some terms are neglected

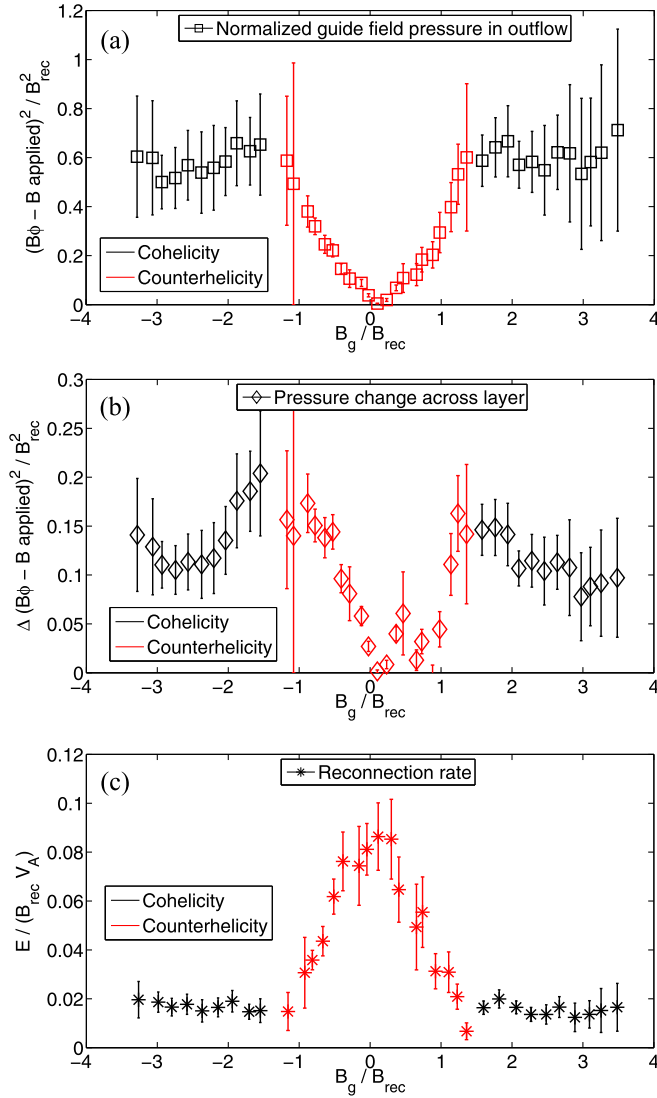


FIG. 6. (a) Total magnetic pressure in the outflow due to the compressed guide field, (b) change in guide field pressure across the layer, and (c) reconnection rate for counterhelicity (red) and cohelicity (black) guide field reconnection. The correlation between the reconnection rate and the magnetic pressure boundary conditions suggests that global effects may play a role in the reconnection dynamics in MRX. (a) Magnetic pressure of the compressed guide field,  $(B_\phi - B_{applied})^2 / 2\mu_0$ , evaluated in the reconnection outflow (8 cm downstream) and normalized to the magnetic pressure of the reconnection field,  $B_{rec}^2 / 2\mu_0$ . (b) Magnetic pressure difference (outflow pressure – inflow pressure) from 7.5 cm upstream to 8 cm downstream of the reconnection x-point as a function of guide field. (c) Reconnection rate as a function of guide field.

when integrating  $J \times B$  into the compressed guide field pressure. However, the gradient  $-\nabla(B_\phi - B_{applied})^2 / 2\mu_0$  has been verified in the present data to be approximately consistent with the locally measured  $J \times B$  force, indicating that this approximation is reasonable for the present discussion.

In Figure 6, we examine some features of the guide field compression which indicate that it may be an important contributing factor to the reconnection rate reduction. The toroidal field compression effects are dominated by large scale structure in the radial direction, while the toroidal field does not vary significantly in  $z$ . As a basic indicator of the magnitude of toroidal field compression effects, Figure 6(a) shows

the total compressed guide field pressure in the reconnection outflow as a fraction of the reconnection field pressure (as determined by the Harris fit). As guide field is added, the toroidal field pressure in the outflow (which opposes reconnection) increases to a substantial fraction of the reconnection field pressure (which drives the reconnection).

This pileup can significantly modify the local profiles of the reconnection layer. Figure 6(b) shows that the compressed guide field produces a local pressure difference across the layer. This difference in pressure is measured from 7.5 cm upstream to 8 cm downstream of the reconnection x-point. This data is somewhat noisier than Figure 6(a), but it shows a similar trend: as the guide field is increased, the compressed field produces a local pressure difference across the layer.

Finally, Figure 6(c) shows the normalized reconnection rate. For counterhelicity plasmas, this drops from its peak (0.08) at zero guide field to a small value (0.02) at guide field  $B_g \approx 1.5B_{rec}$ . This is concomitant with the rise in pressure due to guide field pileup. During cohelicity reconnection, the normalized reconnection rate is consistently small; correspondingly, the guide field pileup pressure is consistently a significant fraction of the reconnection drive. The reconnection rate and guide field compression do not change significantly as guide field is added to cohelicity plasmas; this may be attributed to the fact that global effects in cohelicity plasmas are different from those in counterhelicity plasmas because of differences in their global setup (see Fig. 2). While not conclusive, the correlation between reconnection rate and guide field pressure pileup suggests that modified reconnection boundary conditions imposed by these global effects may play an important role in determining the reconnection rate.

Guide field compression and the associated pressure pile-up is not significant in the simulation. However, this compression is clearly important in at least one respect because the reconnection rates shown in Figure 4 agree only when comparing the simulation results with the local (enhanced) value of the compressed guide field in the experiment. In addition, the reconnection rate may be influenced by the modified boundary conditions to the local reconnection region. Understanding the details of how the guide field pileup quantitatively impacts the local reconnection through boundary condition effects requires new measurements and simulation beyond those currently available, and will therefore be addressed in future work.

## VI. CONCLUSION

In summary, we have systematically produced reconnection in a two-fluid regime with varying amounts of guide field in MRX, and we have compared these results in detail to a Hall MHD simulation with a similarly varied guide field. We observe that the addition of guide field modifies the electron flow, producing similar changes to the quadrupole field structure in the simulation and the experiment. As guide field is added, both the reconnection rate and the size of the Hall terms of Ohm's law are reduced simultaneously, indicating that the electron dynamics are linked to changes in the

reconnection rate. The modified Hall current profile with reduced electron flows in the local reconnection plane quantitatively explains the observed reduction of the reconnection rate.

In addition, we observed a compression of the global guide field, not represented in the Hall MHD simulations. The associated magnetic field pressure alters the boundary conditions of reconnection in MRX in a way not captured by the simulation, yet the reconnection rates agree remarkably well between simulation and experiment as long as the locally enhanced guide field value is used to analyze the MRX data. The strong agreement between simulation and experiment despite differences in the reconnection boundary conditions is suggestive that these boundary effects may not be critical to the reconnection rate in MRX; however, the notable change in the magnetic pressure associated with guide field compression, and the correlation between this pressure and the reconnection rate reduction indicate that this warrants further investigation.

- <sup>1</sup>E. G. Zweibel and M. Yamada, *Annu. Rev. Astron. Astrophys.* **47**, 291–332 (2009).
- <sup>2</sup>M. Yamada, R. Kulsrud, and H. Ji, *Rev. Mod. Phys.* **82**(1), 603–664 (2010).
- <sup>3</sup>J. Berchem and C. Russell, *J. Geophys. Res.* **87**(10), 8139–8148, doi:10.1029/JA087iA10p08139 (1982).
- <sup>4</sup>M. Øieroset, T. D. Phan, M. Fujimoto, R. P. Lin, and R. P. Lepping, *Nature (London)* **412**, 414 (2001).
- <sup>5</sup>J. P. Eastwood, M. A. Shay, T. D. Phan, and M. Øieroset, *Phys. Rev. Lett.* **104**, 205001 (2010).
- <sup>6</sup>J. Egedal, W. Fox, N. Katz, M. Porkolab, K. Reim, and E. Zhang, *Phys. Rev. Lett.* **98**(1), 15003 (2007).
- <sup>7</sup>M. Yamada, H. Ji, S. Hsu, T. Carter, R. Kulsrud, Y. Ono, and F. Perkins, *Phys. Rev. Lett.* **78**(16), 3117–3120 (1997).
- <sup>8</sup>Y. Ono, A. Morita, M. Katsurai, and M. Yamada, *Phys. Fluids B* **5**, 3691 (1993).
- <sup>9</sup>M. Yamada, Y. Ono, A. Hayakawa, and M. Katsurai, *Phys. Rev. Lett.* **65**, 721 (1990).
- <sup>10</sup>T. P. Intrator, X. Sun, G. Lapenta, L. Dorf, and I. Furno, *Nat. Phys.* **5**, 521–526 (2009).
- <sup>11</sup>Y. Yagi and N. Kawashima, *Jpn. J. Appl. Phys., Part 2* **24**(4), L259–L262 (1985).
- <sup>12</sup>A. G. Frank, S. Yu. Bogdanova, G. V. Dreiden, V. S. Markov, and G. V. Ostrovskaya, *Phys. Lett. A* **348**, 318–325 (2006).
- <sup>13</sup>A. Y. Aydemir, *Phys. Fluids B* **4**, 3469 (1992).
- <sup>14</sup>X. Wang and A. Bhattacharjee, *Phys. Rev. Lett.* **70**, 1627 (1993).
- <sup>15</sup>R. G. Kleva, J. F. Drake, and F. L. Waelbroeck, *Phys. Plasmas* **2**, 23 (1995).
- <sup>16</sup>H. Karimabadi, D. Krauss-Varban, N. Omid, and H. X. Vu, *J. Geophys. Res.* **104**(A6), 12313–12326, doi:10.1029/1999JA900089 (1999).
- <sup>17</sup>X. Wang, A. Bhattacharjee, and Z. Ma, *J. Geophys. Res.* **105**(A12), 27633–27648, doi:10.1029/1999JA000357 (2000).
- <sup>18</sup>B. Rogers, R. Denton, J. Drake, and M. Shay, *Phys. Rev. Lett.* **87**(19), 195004 (2001).
- <sup>19</sup>P. L. Pritchett and F. V. Coroniti, *J. Geophys. Res.* **109**, A01220, doi:10.1029/2003JA009999 (2004).
- <sup>20</sup>P. Ricci, J. U. Brackbill, W. Daughton, and G. Lapenta, *Phys. Plasmas* **11**, 4102 (2004).
- <sup>21</sup>J. D. Huba, *Phys. Plasmas* **12**, 012322 (2005).
- <sup>22</sup>M. Swisdak, J. F. Drake, M. A. Shay, and J. G. McIlhargey, *J. Geophys. Res.* **110**, A05210, doi:10.1029/2004JA010748 (2005).
- <sup>23</sup>P. Cassak and J. F. Drake, *Phys. Plasmas* **14**, 054502 (2007).
- <sup>24</sup>C. Huang, Q. Lu, and S. Wang, *Phys. Plasmas* **17**, 072306 (2010).
- <sup>25</sup>M. V. Goldman, G. Lapenta, D. L. Newman, S. Markidis, and H. Che, *Phys. Rev. Lett.* **107**, 135001 (2011).
- <sup>26</sup>A. W. Edwards, D. J. Campbell, W. W. Engelhardt, H.-U. Fahrback, R. D. Gill, R. S. Granetz, S. Tsuji, B. J. D. Tubbing, A. Weller, J. Wesson, and D. Zaslav, *Phys. Rev. Lett.* **57**(2), 210–213 (1986).
- <sup>27</sup>T. D. Tharp, A. F. Almagri, M. C. Miller, V. V. Mirnov, S. C. Prager, J. S. Sarff, and C. C. Kim, *Phys. Plasmas* **17**, 120701 (2010).
- <sup>28</sup>P. Sweet, *Int. Astron. Union Symp.* **6**, 149–176 (1958).
- <sup>29</sup>E. N. Parker, *J. Geophys. Res.* **62**(4), 509–520, doi:10.1029/JZ062i004p00509 (1957).
- <sup>30</sup>H. Ji, M. Yamada, S. Hsu, and R. Kulsrud, *Phys. Rev. Lett.* **80**(15), 3256–3259 (1998).
- <sup>31</sup>J. Birn, J. F. Drake, M. A. Shay, B. N. Rogers, R. E. Denton, M. Hesse, M. Kuznetsov, Z. W. Ma, A. Bhattacharjee, A. Ottos, and P. L. Pritchett, *J. Geophys. Res., [Space Phys.]* **106**(A3), 3715–3719, doi:10.1029/1999JA900449 (2001).
- <sup>32</sup>M. Yamada, Y. Ren, H. Ji, J. Breslau, S. Gerhardt, R. Kulsrud, and A. Kuritsyn, *Phys. Plasmas* **13**, 052119 (2006).
- <sup>33</sup>T. D. Tharp, M. Yamada, H. Ji, E. Lawrence, S. Dorfman, C. E. Myers, and J. Yoo, *Phys. Rev. Lett.* **109**, 165002 (2012).
- <sup>34</sup>E. Harris, *Il Nuovo Cimento* **23**, 115 (1962).
- <sup>35</sup>H. Ji, M. Yamada, S. Hsu, R. Kulsrud, T. Carter, and S. Zaharia, *Phys. Plasmas* **6**(5), 1743 (1999).
- <sup>36</sup>Y. Ren, M. Yamada, H. Ji, S. Dorfman, S. P. Gerhardt, and R. Kulsrud, *Phys. Plasmas* **15**, 082113 (2008).